ChemComm

REVIEW ARTICLE

View Article Online
View Journal

Cite this: DOI: 10.1039/d6cc00216a

Electrochemical C–N coupling: a review of mechanistic pathways and computational frameworks

Jensie Low[a] and Pengfei Ou *[abc]

Received 12th January 2026,
Accepted 30th March 2026

DOI: 10.1039/d6cc00216a

rsc.li/chemcomm

Electrochemical C–N coupling has emerged as a promising strategy for the sustainable synthesis of value-added chemicals derived from carbon- and nitrogen-containing feedstocks, such as CO_2, NO_3^-, NO_2^- and N_2. Despite progress in the field, the selective formation of C–N bonds remains challenging due to the need for the simultaneous activation of both reactants while suppressing the competing reaction pathways. Recent computational advances, including periodic density functional theory, grand-canonical and constant-potential methods, and data-driven catalyst screening, have enabled improved mechanistic insights. These computational approaches have allowed the rational design of catalysts capable of co-stabilising the carbon and nitrogen intermediates and promoting preferential C–N coupling over competitive product formation. This review will highlight the current understanding of the mechanistic and computational methods that drive the current discovery of the catalysts capable of efficient electrochemical C–N coupling.

1. Introduction

The rise in atmospheric concentrations of carbon dioxide (CO_2) and reactive nitrogen species, such as nitrate (NO_3^-), nitrite (NO_2^-), and molecular nitrogen (N_2), has intensified the search for promising sustainable strategies to transform these abundant feedstocks into value-added products, including urea, carbamates, and amides, through electrochemical C–N coupling. Compared with conventional thermodynamic routes,

[a] Department of Chemistry, National University of Singapore, 3 Science Drive 3, Singapore, 117543, Singapore. E-mail: pengf.ou@nus.edu.sg
[b] NUS Artificial Intelligence Institute, National University of Singapore, 11 Research Link, Singapore, 119391, Singapore
[c] Centre for Hydrogen Innovations, National University of Singapore, 1 Engineering Drive 3, Singapore, 117580, Singapore

Jensie Low

Jensie Low received her BSc degree (Chemistry) in 2023 from the National University of Singapore. Thereafter, she obtained her joint MSc degree in Nanoscience and Nanotechnology from KU Leuven and Université Grenoble Alpes in 2025. She is currently pursuing her PhD degree at the National University of Singapore, with her research focusing on the computational modelling of reacting catalytic systems and ML/AI techniques for chemical research.

Pengfei Ou

Pengfei Ou received his BE and ME degrees in Materials Science and Engineering from the Central South University in 2012 and 2015, respectively. He then obtained his PhD degree from the McGill University in 2020. During 2020–2022 and 2022–2024, he was trained as a postdoctoral fellow at the University of Toronto and as a Research Associate at the Northwestern University. Subsequently, he joined the National University of Singapore in 2024 as an Assistant Professor. His current research primarily focuses on computational catalysis, electrochemistry, machine learning, and AI for Science.

such as the Bosch–Meiser process, wherein the reaction proceeds at a high temperature and high pressure,[1] the electrochemical pathway offers potential to synthesise these products under ambient conditions while mitigating greenhouse gas emissions.

Despite this promise, selective C–N coupling remains challenging due to the kinetic inertness of both the carbon and nitrogen reactants and the synchrony of the reduction pathways, which must occur at the catalyst-electrolyte interface. CO_2 reduction is thought to proceed typically through the formation of *COOH and its subsequent conversion into *CO.[2] In parallel, nitrogen activation occurs simultaneously through multi-electron pathways, with its mechanism dependent on the nitrogen source and catalyst used. For NO_3^- and NO_2^-, the reduction can involve $*NO_2$, *NO, *HNO, and $*NH_2$ intermediates,[3] but the preferred pathway and branching are catalyst-dependent.[4] In the case of N_2 as the feedstock, N_2 first requires adsorption, followed by electron donation into the antibonding orbitals to weaken the $N\equiv N$ triple bond.[5] Successful C–N coupling occurs only when these reductions occur in parallel and converge to compatible intermediates; for instance, *CO and $*NH_2$ intermediates are key to the formation of $*CONH_2$.

Achieving this convergence is critically dependent on catalyst design. Effective materials must be designed to offer bifunctional or spatially cooperative sites capable of stabilising both carbon- and nitrogen-derived intermediates while suppressing the competing pathways, most notably hydrogen evolution. In recent years, single-atom[6,7] and double-atom[8] catalysts, MXenes,[9] MBenes[10] and other 2D heterostructures, amongst others, have highlighted how tuneable coordination and local electronic environments can critically steer intermediate binding and, ultimately, C–N selectivity.

Computational modelling has been an essential tool in guiding the development of appropriate catalysts. Density functional theory (DFT) is consistently used to quantify adsorption energies, construct the free-energy landscape, identify potential-determining steps, elucidate reaction mechanisms, and provide an improved overall understanding of how catalysts govern C–N coupling selectivity. Beyond conventional DFT workflows, machine learning–accelerated DFT, high-throughput screening, and descriptor-based frameworks have enabled the expansion of the search for active materials and simplified the identification of new candidates for C–N coupling reactions.

In this review, we offer a summary of C–N coupling reaction pathways and summarise recent computational techniques for understanding and predicting electrochemical C–N coupling with an emphasis on mechanistic modelling and descriptor development for accelerated catalyst discovery.

2. Overview of electrochemical C–N coupling

Electrochemical C–N coupling enables the conversion of carbon and nitrogen feedstocks, such as CO_2, N_2, NO_3^-, NO_2^-, and NH_3, into value-added chemical products, including urea,[3] carbamates,[11] acetamide,[12] and amides.[13] The coupling reaction typically involves four stages: (i) the adsorption of carbon- and nitrogen-containing reactants onto the catalyst surface, (ii) activation of key intermediates through proton-coupled electron transfer (PCET) to generate reactive intermediates, (iii) C–N bond formation between intermediates suitably positioned with respect to each other, and (iv) the desorption of the C–N formed product. A balance of the interaction strength between the adsorbates and the catalyst must be achieved such that the intermediate reacts strongly enough to undergo subsequent PCET steps but not too strongly such that the individual feedstocks become fully reduced to form, *e.g.*, CO_2 to CH_4 (eqn (1))[14] and N_2/NO_x to NH_3 (eqn (2)–(4)),[15–17] which leads to the suppression of C–N coupling as follows:

$$CO_2 + 8H^+ + 8e^- \rightarrow CH_4 + 2H_2O \quad (1)$$

$$N_2 + 6H^+ + 6e^- \rightarrow 2NH_3 \quad (2)$$

$$NO_3^- + 9H^+ + 8e^- \rightarrow NH_3 + 3H_2O \quad (3)$$

$$NO_2^- + 7H^+ + 6e^- \rightarrow NH_3 + 2H_2O \quad (4)$$

2.1. CO_2 activation and reduction pathways

CO_2 is a linear, thermodynamically stable molecule that can undergo surface adsorption in multiple configurations. While CO_2 can directly react with nitrogen-containing intermediates before undergoing any form of hydrogenation (Fig. 1),[4] it typically undergoes some form of activation into other key intermediates, such as *CO. For instance, on the Ni triple atom-doped Cu_2O catalyst, preferential adsorption through the carbon atom is observed, consistent with the carbon affinity at Ni sites.[5] The adjacent oxygen atoms can also form a bond with the catalyst surface, resulting in the ''lying-down'' configuration. Upon adsorption, CO_2 often deviates from linearity, facilitating stronger orbital mixing between CO_2-derived states (C 2p orbitals) and the surface metals (Ni/Cu 3d orbitals), which can be examined through projected density of states (pDOS) analysis. As the stability of the molecules on the catalyst surface is primarily determined by their binding strengths, this interaction, which represents the hybridisation of the electronic structures, can be attributed to the stabilisation of the adsorbed CO_2.

Once adsorbed, bent CO_2 can undergo reduction *via* PCET to form *COOH, followed by the dehydration to yield *CO, as shown in Fig. 1.[2,18,19] The binding strengths of the *COOH and *CO intermediates to the catalyst are crucial: overly strong *CO binding can lead to site blocking (surface poisoning) and suppress subsequent C–N coupling, whereas weak binding may cause premature desorption before coupling can occur.

2.2. Activation of nitrogen species

Having summarised CO_2 activation, the activation of several nitrogen species will now be discussed. Several nitrogen-containing feedstocks can participate in electrochemical C–N coupling, including N_2, NO_3^-, NO_2^-, and NO. While NH_3 can, in principle, act as a feedstock, it is less common as it is already

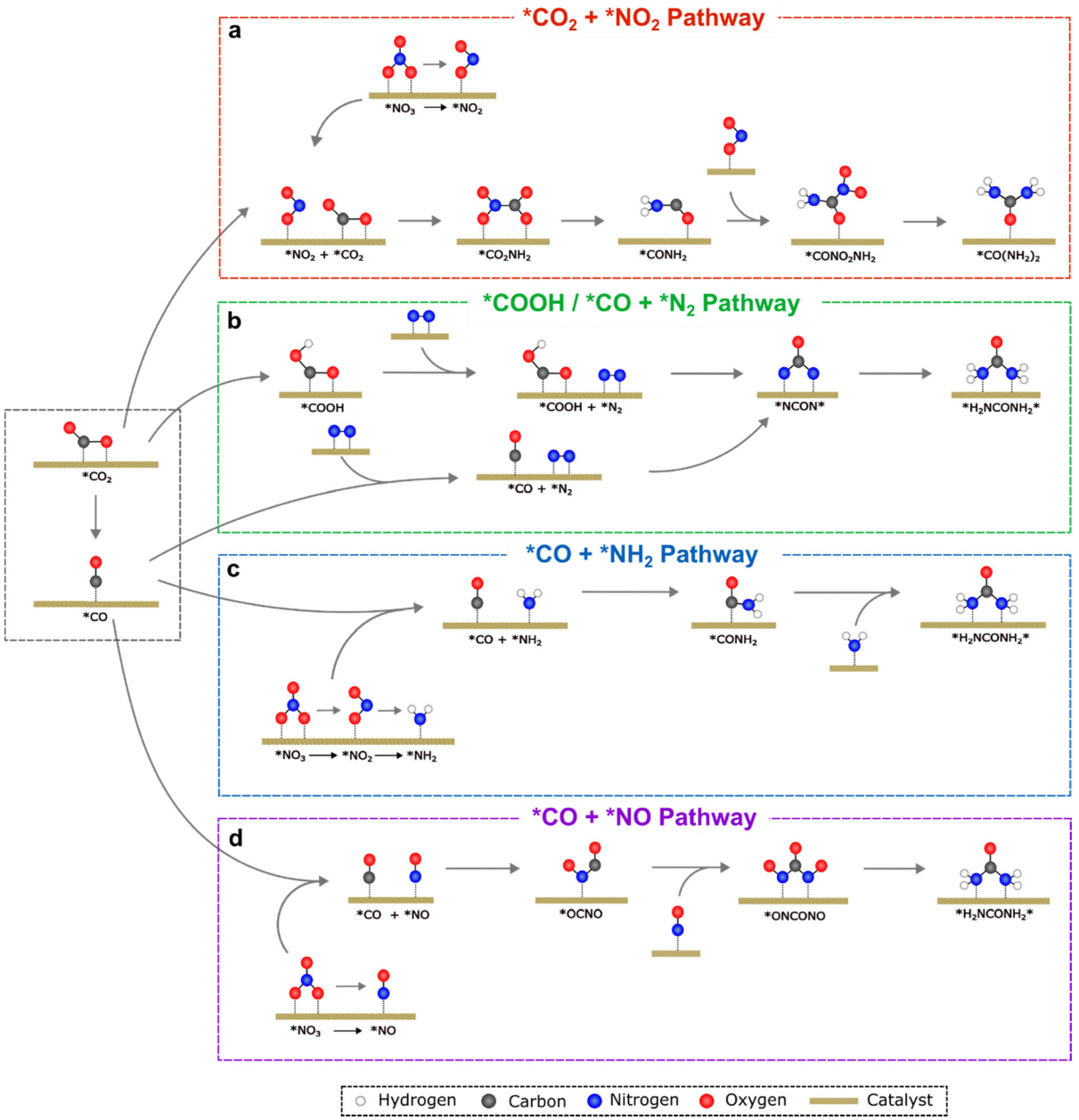

Fig. 1 C–N coupling reactions with different nitrogen-based reactants, resulting in the formation of urea. *CO_2 + (a) *NO_2, (b) *N_2, (c) *NH_2 and (d) *NO. Panels (a), (c), and (d) are adapted from ref. 20, with permission from Wiley-VCH GmbH, copyright, 2024. Panel (b) is adapted from ref. 21, under the terms of the CC BY 4.0 license. The pathways shown are representative mechanisms reported in the literature and are not exhaustive.

a fully reduced nitrogen species and, therefore, exhibits limited electrophilicity compared to its counterparts.

2.2.1. Nitrate, nitrite, and nitric oxide reduction. From a practical perspective, NO_3^- and NO_2^- are attractive nitrogen sources as they can adsorb strongly on the catalyst surface and are capable of undergoing multi-electron PCET steps to form *NH_2, a widely discussed coupling-competent intermediate. Depending on the catalyst, earlier NO_x-derived intermediates (*e.g.*, *NO or *NO_2) may also participate directly in the coupling (Fig. 1). In addition, NO_3^-/NO_2^- species are often more readily activated than N_2 because N_2 activation must first overcome the inert N≡N triple bond. The nitrate reduction reaction (NO_3RR) and nitrite reduction reaction (NO_2RR) often share a similar hydrogenation sequence, which can be written as follows:

$$NO_3^- \rightarrow *NO_2 \rightarrow *NO \rightarrow *NHO \rightarrow *NH_2O \rightarrow *NH_2 \quad (5)$$

Once formed, *NH_2 can couple with *CO to generate C–N intermediates *en route* to products, such as urea or amides. However, if *NH_2 bonds too strongly, complete hydrogenation to NH_3 is favoured, which typically reduces coupling propensity under many conditions. In many reported systems, the overall rate is sensitive to the nitrogen-side hydrogenation, and the

rate-determining step (RDS) can vary with the active motif. For instance, for the Ni–O–C interface,[2] the *NO → *NHO step has been proposed as the RDS, whereas the RDS on TAC@Cu_2O is reported as *CO + *N_2 + H^+ + e^- → *CONNH.[2,5] These studies show that there is no one-size-fits-all description for understanding the C–N coupling reactions; instead, catalyst-specific computations are typically required to map the dominant pathway and kinetic bottlenecks. While less reported, in the case of nitric oxide (NO) as a feedstock, NO will first similarly undergo hydrogenation (eqn (5)) till *NH_2 is formed before undergoing a coupling reaction.[22]

2.2.2. N_2 activation. When N_2 is used as the nitrogen source, its strong triple bond requires a suitable catalyst that facilitates adsorption and back-donation. DFT studies across diverse catalyst families, including MBenes,[10] Ni triple-atom-doped Cu_2O electrocatalysts,[5] Mo_2P monolayer,[21] and B12@C2N catalysts,[23] have been conducted. While other mechanisms exist, in these studies, N_2 exhibits preferential side-on adsorption on the catalyst surface due to back-donation of electrons from the metal d-orbitals into the N_2 π* antibonding orbitals. Upon N_2 adsorption, the elongation of the N–N bond is typically observed, indicating bond weakening and enabling subsequent PCET steps. A commonly discussed route to urea formation couples activated N_2-derived intermediates with CO_2 reduction intermediates. One illustrative sequence is as follows:[5,23]

$$N_2 + CO_2 \rightarrow {}^*N_2 + {}^*CO_2 \rightarrow {}^*N_2 + {}^*COOH \rightarrow {}^*N_2 + {}^*CO \rightarrow {}^*NCON \rightarrow {}^*NCONH \rightarrow {}^*NHCONH \rightarrow {}^*NHCONH_2 \rightarrow {}^*NH_2CONH_2 \quad (6)$$

The above pathway shows the formation of NCON, beginning with the insertion of *CO into activated *N_2 to form a tower-like species, *NCON, where the two nitrogen atoms are bonded to the catalyst surface.[23] The *NCON intermediate then undergoes successive hydrogenation to yield hydrogenated intermediates before ultimately producing a C,N-product, such as urea (eqn (6)).

The detailed pathway and preferred coupling intermediate depend strongly on the surface electronic structure and the relative stability of competing hydrogenation steps; therefore, it is important to acknowledge that not all possible reaction mechanisms are covered here. Fig. 1 summarises representative mechanistic possibilities for urea formation starting from CO_2 and N_2.

3. Competitive pathways

Beyond the reactions of interest, it is prudent to discuss the commonly occurring competing pathways when discussing C–N coupling. Electrocatalytic C–N coupling inevitably competes with parallel reactions that consume key intermediates, diverting them to form other products than the desired output. The major competing reactions are the hydrogen evolution reaction (HER), CO_2 reduction reaction (CO_2RR) to form formate or methane, and the over-reduction of nitrogen intermediates to ammonia. Understanding competing reactions will enable the design of catalysts because selectivity is determined by how the catalyst stabilises carbon- and nitrogen-derived intermediates relative to hydrogen adsorption and sequential hydrogenation chemistry.

3.1. Hydrogen evolution reaction

The HER occurs on catalysts that convert protons (H^+) or water molecules into molecular hydrogen (H_2). Generally, several elementary steps occur; first is the adsorption of hydrogen onto the catalyst surface to form *H. Second is the combination of adsorbed hydrogen into H_2, and the final step is the desorption of H_2 from the surface. The elementary adsorption of hydrogen onto the catalyst depends on the nature of the environment, whether acidic or alkaline.[24]

Under acidic conditions,

$$H^+ + e^- \rightarrow H^* \quad (7)$$

Under alkaline conditions,

$$H_2O + e^- \rightarrow H^+ + OH^- \quad (8)$$

Under alkaline conditions, breaking the O–H bond is required, resulting in an intrinsically slower reaction. The second step can then occur either through electrochemical desorption, where an adsorbed H* reacts with another proton/electron to form H_2, which again depends on the environment:

Under acidic conditions,

$$H^* + H^+ + e^- \rightarrow H_2 \quad (9)$$

Under alkaline conditions,

$$H^+ + H_2O + e^- \rightarrow H_2 + OH^- \quad (10)$$

Alternatively, a chemical combination of two adsorbed hydrogen atoms can occur on the catalyst surface as follows:

$$H^* + H^* \rightarrow H_2 \quad (11)$$

While several methods to suppress the HER exist,[25] the most common and straightforward is to make hydrogen adsorption unfavourable. When the catalyst binds too weakly to the catalyst, the electron transfer between H^+ and the catalyst becomes unfavourable. In addition to reducing the hydrogen affinity, catalysts can be designed to bind preferentially to the desired reactants, such as Cu, which favours strong *CO binding and moderate H binding, and Ni, which prefers *N_2 binding over H binding.

3.2. Formate formation

On the carbon side, C–N coupling often relies on the generation of *CO or other coupling competent C_1 intermediates from CO_2RR. A key branching point is the first CO_2 hydrogenation. If *COOH is not formed, the C–N product yields decrease as the C–N coupling reaction is inhibited. The formate formation pathway is one that can compete with and prevent the formation of *COOH. To form formate, CO_2 reacts with a proton to

form *OCHO, which can then desorb to form the undesired formate, $HCOO^-$.

The mechanistic difference between forming *COOH and *OCHO is determined by the atom bound to the active site. Chemically, they both undergo the reaction: $CO_2 + H^+ + e^- \rightarrow$ *COOH; however, to form *COOH, the carbon atom of CO_2 binds the surface, whereas *OCHO formation proceeds through the hydrogenation of oxygen-bound CO_2.[26,27] The relative stability and binding strength of these intermediates on different metal surfaces largely govern product selectivity: surfaces that tend to stabilise *OCHO relative to *COOH favour formate, whereas surfaces that favour *COOH binding favour CO evolution.[28] Thus, catalyst design strategies should focus on tuning surface properties to favour C-bound adsorption over O-bound adsorption, for instance, by decreasing the oxophilicity or modifying the electronic structure of the surface to destabilise oxygen-bound intermediates.

3.3. Ammonia and methane formation

Over-reduction of nitrogen intermediates is another major channel for selectivity loss that competes directly with C–N bond formation. When $*NH_2$ binds too favourably to the catalyst or when *CO binding is too weak and does not promote co-adsorption, the system favours the continued hydrogenation of nitrogen intermediates to ammonia, resulting in a reduced faradaic efficiency (FE) of the C–N product formation. This issue is prevalent in catalysts with isolated active sites, such as some single-atom catalysts (SACs) that do not promote co-adsorption, decreasing the likelihood of timely coupling before complete hydrogenation occurs.

A similar issue occurs on the carbon-derived intermediate. Excessively strong binding of *CO may lead to further hydrogenation to methane, consuming both electrons and protons, thereby preventing the C–N coupling pathway that relies on the availability of *CO. Conversely, if *CO binds too weakly, it may desorb before it can encounter a nitrogen-derived partner on the surface. Overall, optimal catalysts for selective C–N coupling typically require (i) moderate binding of the carbon- and nitrogen-derived intermediates, (ii) co-adsorption capability for both carbon- and nitrogen-derived intermediates, and (iii) the prevention of unwanted further hydrogenation pathways.

4. Catalytic platforms and material designs

Achieving high selectivity of the desired products over the competitive side reactions, as discussed prior, is largely dependent on the catalyst. Therefore, a wide variety of catalyst classes will now be discussed. Different classes of catalysts have been explored to overcome the challenge of simultaneous activation of carbon- and nitrogen-containing species for C–N bond formation. These catalysts differ in their geometric structures, electronic configurations, nature of their active sites, and ability to promote co-adsorption and spatial proximity among key intermediates. In this section, we summarise the major catalyst classes investigated for C–N coupling, including single-atom, dual-atom catalysts, two-dimensional materials, molecular catalysts, metal-based catalysts and porous frameworks.

4.1. 2D material-based platforms

Catalyst design strategies, such as single-atom catalysts (SACs), dual-atom catalysts (DACs), functionalised MXenes and MBenes, have emerged as promising platforms for electrochemical C–N coupling due to their high atom efficiency, tuneable electronic structures, and ability to stabilise key reaction intermediates.[29,30] These catalysts enable precise control over active sites, which is crucial for simultaneous CO_2RR and NRR.

SACs (Fig. 2a) are popular heterogeneous catalysts composed of individually isolated metal atoms dispersed on a support surface rather than forming clusters or nanoparticles. SACs represent the highest possible atom efficiency since each atom serves as an active catalytic site. Several SAC systems have demonstrated the ability to enhance electrochemical reactions, including C–N coupling. One such system is the Cu–N–C SAC system,[18] which contains both sites active for CO_2RR and NO_3RR, achieving a FE of 28% for urea production with a current density of -27 mA cm^{-2} at -0.9 V *vs.* RHE. It has previously been shown that in SACs, the atoms surrounding isolated metal atoms may also exhibit catalytic activity[6,7] and, therefore, affect selectivity. This is also observed in the case of the Cu–N–C catalyst. When the number of N atoms bonded to Cu decreases and the atoms are replaced by the C atom, the selectivity preference shifts from CO_2RR to NO_3RR. However, this may not always be the case, and some SACs prefer only CO_2RR or nitrogen reduction reaction (NRR), which is not ideal in C–N coupling, as both must occur simultaneously.[8] Dual-atom catalysts are therefore designed to counter this limitation of SACs.

The design of dual-atom catalysts (Fig. 2b) addresses the limitations of their SAC counterparts, enabling CO_2RR and NRR to occur synergistically. The Ni–Mo diatomic catalytic system (NiMo-DASC) is one such system that offers dual active sites and is capable of urea electrochemical synthesis.[8] It was designed in such a manner that the Mo sites exhibit enhanced activity towards NO_3RR and the Ni sites have a preference towards CO_2RR. The two metal atoms, therefore, demonstrate a synergistic relationship towards the synthesis of urea. The authors reported an FE of 31.8% and a yield of 11.3 mmol g^{-1} h^{-1}, while the SAC counterpart (Mo-SAC and Ni-SAC) exhibited a lower urea FE and yield, attributed to the lower CO_2RR and NO_3RR activities.

In parallel, 2D materials, such as functionalised MXenes, have been gaining popularity as catalysts due to their large surface area, tuneable electronic structures and abundant surface active sites.[29,30] MXenes are typically composed of transition-metal carbides or nitrides with properties such as metallic conductivity and surface groups, which can be altered according to the desired needs, such as to stabilise the C and N intermediates during a C–N coupling reaction. MBenes are the boride-based analogues of MXenes, which offer unique metal-boron interactions that promote charge transfer and bond

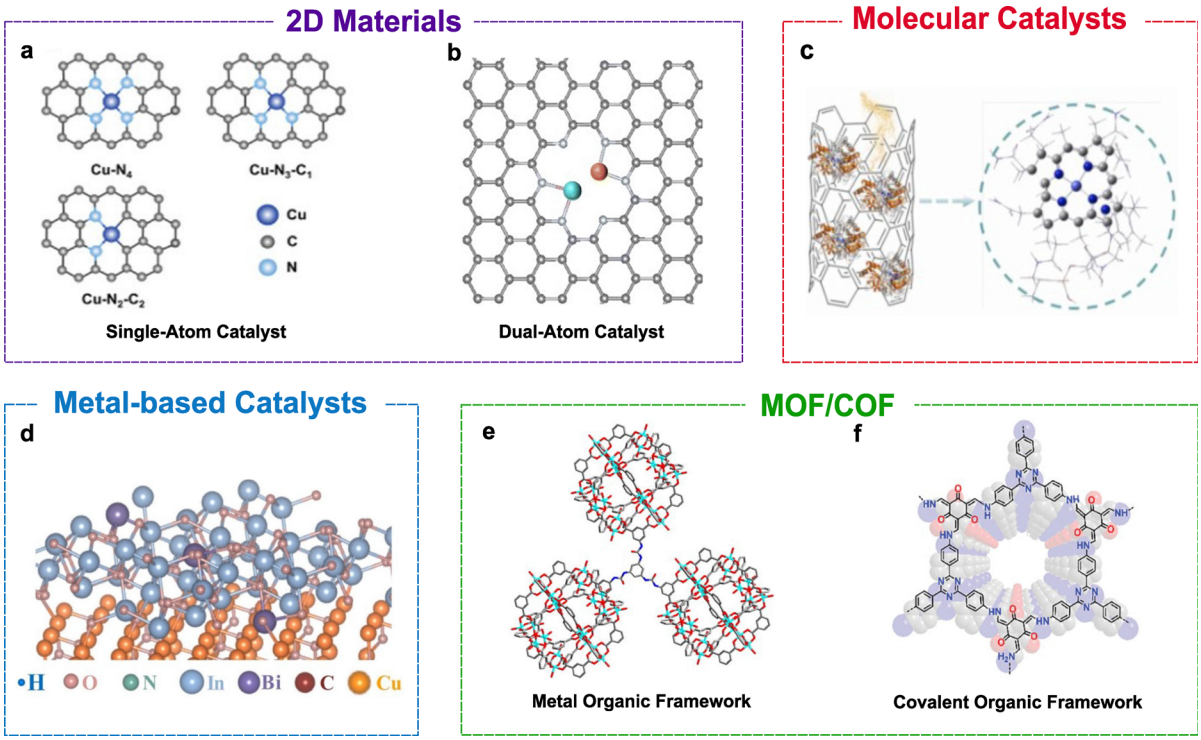

Fig. 2 Representative catalyst classes for electrochemical C–N coupling: (a) single-atom catalysts, adapted from ref. 18, under the terms of the CC BY 4.0 license; (b) dual-atom catalysts, adapted from ref. 8, under the terms of the CC BY 3.0 license; (c) molecular catalysts, adapted from the ref. 31, with permission from Elsevier B.V., copyright, 2024; (d) p-doped metal-based catalysts, adapted from ref. 32, with permission from Elsevier B.V., copyright, 2025; (e) metal–organic frameworks, adapted from ref. 33, with permission from Elsevier Ltd., copyright, 2025; and (f) covalent organic frameworks, adapted from ref. 34, with permission from Wiley-VCH GmbH, copyright, 2025. In all cases, the original figures were cropped to show only the catalyst structures.

activation. 2D materials offer atomic thinness and the possibility for defect and surface group engineering, allowing control over desired reaction pathways. These properties make 2D materials promising materials for C–N bond formation.

4.2. Molecular catalysts

Several molecular catalysts (Fig. 2c) have been studied for CO_2RR, NRR and C–N coupling as they offer coordination environment precision.[11] Transition metal complexes are some of the most common molecular catalysts capable of selective activation through redox reaction. Through the alteration of the ligands, the electronic structure of the catalyst can be modified and tuned to stabilise key intermediates. A recent work by Cong *et al.* (2024) demonstrated that natural vitamin B12 molecules immobilised on carbon nanotubes are capable of catalysing the electrochemical C–N coupling between CO_2 and nitrate to produce urea.[31] Vitamin B12 is a large organometallic molecule with a cobalt ion embedded within a corrin ring. A FE of 26.04% at −0.5 V *vs.* the RHE was achieved, with a production yield of 164.04 μg h^{-1} mg^{-1} and a turnover number (TON) of 830.53, demonstrating the ability of molecular catalysts for C–N coupling with the right catalyst design.

4.3. Metal-based catalysts

Metals are another versatile class of catalysts known for their ability to catalyse different types of reactions, including C–N coupling. Monometallic copper, for instance, has shown the capability to catalyse the CO_2RR and promote C–C coupling reactions, and it is also capable of facilitating C–N coupling reactions.[35–37] Despite this, monometallic Cu catalysts have slow reaction kinetics. In a study, CuO*x* was compared to CuO*x*/BiO*x* to study the impact of incorporating p-block metal oxides, potentially providing dual active sites and thereby improving the selectivity towards C–N synthesis over C–C coupling and the HER.[38] The study found that both catalysts were capable of producing formamide; however, the yields between them varied greatly, with 1.4 ± 0.2 mmol h^{-1} g^{-1} for CuO*x* and 2.8 ± 0.3 mmol h^{-1} g^{-1} for CuO*x*/BiO*x* at −1.0 V *vs.* RHE, showing that the addition of a p-block oxide does affect the production of C–N coupled products. The FE reported, however, was low due to the formation of other side products. Nevertheless, this study demonstrates the capability of dual metal oxides to generate the desired C–N products.

4.4. Porous frameworks

Covalent organic frameworks (COFs) and metal organic frameworks (MOFs) are integrated catalytic frameworks, which are highly porous ordered materials that have built-in active sites (Fig. 2e and f) able to host and co-activate both carbon and nitrogen derivatives for C–N coupling. Therefore, they can be considered promising C–N coupling catalysts.[39,40] In the study by Tan *et al.* (2025), a porphyrin-only MOF and a

metalloporphyrin (Cu-porphyrin) MOF were able to react with different levels of NO_3^- which altered the MOF's binding strength to NO_3^- and CO_2 intermediates, enabling the formation of urea. In another study by Liu *et al.* (2025), porphyrin-based COFs were shown to reduce CO_2 and nitrite into urea in the absence of any metals in the catalyst.[41] The metal-free COF features high porosity and strong CO_2 adsorption, facilitating the simultaneous activation of CO_2 and nitrite at a rate of $\approx$0.32 μmol h^{-1}; other side products, such as NH_3, HCOOH and CO, are also formed within the COF. These studies show that both MOFs and COFs are capable of C–N coupling reactions.

5. Computational approaches

Computational methods are commonly employed to better understand the effects of catalysts at the molecular scale. Computational modelling is a key technique for studying the electrochemical C–N coupling as it provides atomistic-level insights into adsorbate binding, reaction energetics, and pathway competition across various catalysts. To date, the most widely used approach is DFT, which can identify key intermediates, quantify their adsorption free energies, locate transition states, and map plausible reaction mechanisms and selectivity trends. Increasingly, periodic DFT is supplemented by electrochemical models (*e.g.*, the computational hydrogen electrode (CHE) model and grand-canonical/constant-potential DFT (GC-DFT/CP-DFT) formalisms) and solvation treatments to better approximate the electrified solid–liquid interface.

5.1. Periodic density functional theory

Periodic DFT remains one of the most influential approaches for mechanistic analysis in heterogeneous electrocatalysis. Periodic DFT utilises Bloch's theorem and periodic boundary conditions to model the electronic structure of crystalline systems. The repeating unit cell of the system is regarded as an infinite lattice, allowing for an accurate simulation of the bulk material and the surface using a plane-wave basis set. In periodic DFT, the ground state energy of a crystalline system is found by using an iterative method to minimise the overall electronic energy (E) of the system. In the CO_2RR and NRR catalytic reactions, periodic DFT is used to compute the adsorption energies of carbon- and nitrogen-derived intermediates, elucidate the reaction mechanism, evaluate transition states, and assess the electronic structures of the catalytic surface.[42–44] These calculations can be performed under vacuum or implicit electrochemical conditions to better mimic experimental conditions.[5]

A practical limitation is that mechanistic exploration is often still manual and combinatorial: for each catalyst, multiple adsorption motifs, intermediate coverages, and candidate pathways must be enumerated and evaluated to identify the most plausible mechanism (*e.g.*, the lowest-barrier or lowest-free-energy route). This challenge becomes particularly acute for C–N coupling, where two reduction manifolds (carbon and nitrogen) must proceed concurrently and sufficient coverage of specific co-adsorbed intermediates is required (Fig. 3a).

The results from periodic DFT calculations can thereafter be used to compare different catalysts within and outside the catalytic class. Standard periodic DFT operates with a fixed electron number and under vacuum conditions, which do not directly correspond to the electrochemical potentials or solvated interfaces that occur experimentally. Therefore, additional approaches, such as the CHE model, GC/CP-DFT, and solvation models, can be used to obtain results more closely aligned with those of experimental design.

5.2. Exchange–correlation functionals and accuracy considerations

The type of exchange–correlation functional used during the DFT calculation influences the accuracy and, therefore, the reliability of adsorption energies, charge transfer, and barrier heights. While higher accuracy is usually preferred, highly accurate techniques incur exponentially higher computational cost. Therefore, a balance between computation cost and accuracy must be achieved when performing DFT and other computational studies. Generalised gradient approximation (GGA) functionals, namely Perdew–Burke–Ernzerhof (PBE)[22,23,45] and revised PBE (RPBE)[46] from Hammer *et al.*, are among the most widely used because they balance computational cost and accuracy. Nevertheless, GGA may underestimate the binding of adsorbates to the catalyst and may misrepresent the localisation of transition-metal d electrons.[47] In these cases, meta-GGA functionals, such as Strongly Constrained and Appropriately Normed (SCAN), or hybrid functionals, such as Perdew–Burke–Ernzerhof hybrid functional (PBE0), can provide improved accuracy for systems in which electron correlation may play an important role.[48–50] Such catalysts may include metal oxides or metal-based SACs, where localised states and charge transfer are central to reactivity.

Due to the functional dependence of deviations in DFT calculations, benchmarking is essential. Even small deviations of 0.1–0.3 eV across functionals may lead to differences in predicted selectivity. Therefore, when it comes to mechanistic studies of C–N coupling, where competing pathways are closely spaced in free energies, the importance of an appropriate functional cannot be understated.

5.3. Solvation and electrolyte models

The electrochemical C–N coupling reaction frequently occurs in aqueous environments, where both CO_2 and nitrogen-derived intermediates interact strongly with water molecules *via* hydrogen bonding and field-stabilised polarisation. Therefore, conventional vacuum DFT is insufficient to accurately represent these effects and misestimates adsorption energies, leading to mispredictions of reaction selectivity. As a result, the representation of the solid–liquid interface is an important challenge that DFT simulations must overcome. To address these challenges, several solvation strategies have been developed and are currently used.

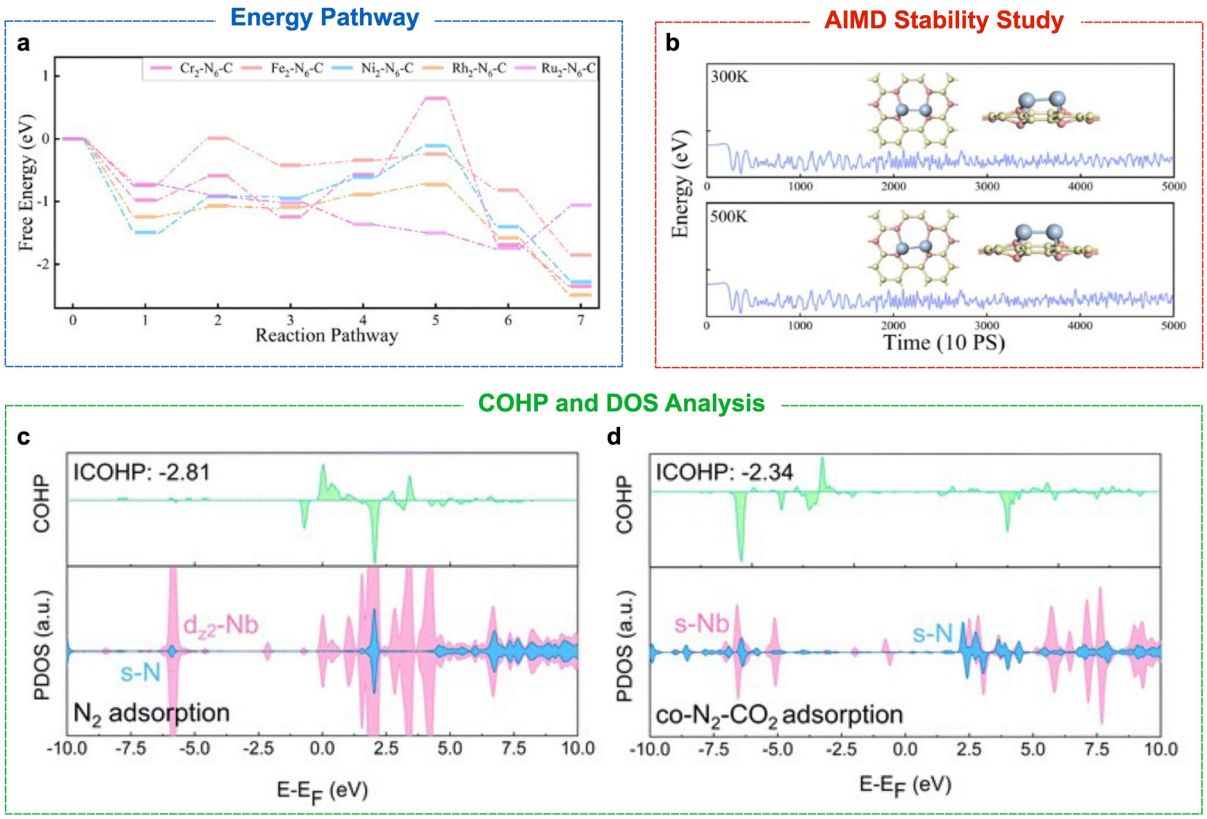

Fig. 3 Computational techniques used for the study of the electrochemical C–N coupling. (a) Static DFT free-energy profiles for the nitrogen reduction reaction (NRR) on several M_2–N_6–C catalysts. (b) AIMD simulations showing the variation of energy with time on the Ru_2–N_6–C surface at 300 and 500 K. Insets: Optimised geometries after AIMD simulations. (c) and (d) COHP and pDOS analyses of Nb@C_2N with N_2 adsorption and the co-adsorption of N_2 and CO_2. Panels (a) and (b) are adapted from ref. 66, with permission from Elsevier B.V., copyright, 2025. Panels (c) and (d) are adapted from ref. 67, with permission from the Royal Society of Chemistry, copyright, 2025. In both cases, the original figures were cropped to show only the panels relevant to the present discussion.

In implicit solvation approaches, such as VASPsol[51] and SCCS,[52] the electrolyte is treated as a polarisable dielectric continuum. Using these methods, solvation energies can be estimated without significantly increasing the computational cost. These implicit models capture long-range polarisation, but they may lack an accurate representation of directional hydrogen bonding and explicit proton-donor/acceptor behaviour, both of which are crucial for PCET kinetics and C–N coupling selectivity. These limitations can be partially addressed by using hybrid implicit–explicit solvation models.[53] The first solvation shell is modelled explicitly using water molecules arranged in multilayer configurations, while the rest of the solvent continues to be represented by a dielectric continuum. With this approach, both localised hydrogen-bonding and proton-transfer behaviours can be captured while maintaining tractable computational costs.

5.4. Computational hydrogen electrode model

The computational hydrogen electrode (CHE) model introduced by Nørskov *et al.* provides a practical means to evaluate PCET steps without explicitly modelling solvated protons and electrons.[54,55] The core of CHE lies in thermodynamic substitution. Instead of separately treating the chemical potentials of H^+ in solution and an electron at a specific potential, the model uses the equilibrium condition $H^+ + e^- \leftrightarrow 1/2\ H_2$ at 0 V against RHE. This allows $(H^+ + e^-)$ to be replaced with $1/2\ H_2$. Consequently, the free-energy changes for the PCET step can be computed directly from DFT-obtained energies, corrected by the free energy of $1/2\ H_2$ and the applied potential.

The free energy of a PCET step at potential U is then expressed as $\Delta G(U) = \Delta G^{\circ}_{\mathrm{DFT}} - eU$, where $\Delta G^{\circ}_{\mathrm{DFT}}$ is the zero-point energy and entropy corrections, and $-eU$ is the energy gained by the external potential U. This correction allows the simple construction of potential-dependent free-energy diagrams, thereby allowing the identification of thermodynamically favourable pathways and potential-determining steps (PDS).

CHE is, however, inherently a thermodynamic model and does not treat charge redistribution explicitly under applied potentials, potential-dependent solvation or explicit electron transfer. For highly polar or charged intermediates, CHE's simplifications may become insufficient, necessitating more advanced methods, such as GC-DFT or CP-DFT.

5.5. Grand-canonical density functional theory

Up to now, only classical DFT methods have been discussed, which are performed at a fixed electron number; thus, the

electronic structure of the catalyst determines the Fermi level and does not correspond to experimentally applied potentials. In GC-DFT, the number of electrons (N) in a simulation cell is allowed to fluctuate in response to an external electron chemical potential (μ_e, a proxy for the electrode). This allows the study of catalytic systems under an applied potential, mimicking the experimental conditions where the grand potential, $\Omega = E - \mu_e N$, is minimised.[56] During the calculation, electrons are added or removed to satisfy an applied μ_e, where the surface charge and local electric field then respond self-consistently. This framework, therefore, captures key electrostatic effects that are difficult to represent in fixed-charge calculations.

CP-DFT represents a practical implementation of the GC-DFT formalism. In most DFT methods, calculations are performed in a canonical ensemble with fixed electron numbers.[57] In CP-DFT, the electron count is adjusted iteratively until the computed Fermi level matches a target electrode potential referenced to a chosen experimental scale, such as the reversible hydrogen electrode (RHE). When combined with implicit solvation models, CP-DFT can reproduce a realistic electrochemical environment in which the surface charge varies naturally with the applied potential, thereby capturing the physics of electrochemical polarisation.

For electrochemical C–N coupling reactions, including those relevant to CO_2RR and NRR, GC- and CP-DFT provide critical insight into potential-dependent reaction behaviours that are inaccessible using fixed-charge DFT or thermodynamic approaches, such as the CHE method.[10,58] Many reaction intermediates involved in these processes are charged or highly polar, and their adsorption energies can vary by several electron volts as a function of the electrode potential.[59] As a result, the relative stability of intermediates, as well as the competition between hydrogenation, desorption, and C–N coupling pathways, is strongly influenced by the applied potential.

Furthermore, the GC-DFT framework allows the investigation of the electric field on reaction transition states. This is particularly important for C–N bond formation steps, which often involve highly polarised transition states with substantial dipole moments. The stabilisation and de-stabilisation of such transition states by the interfacial electric field can significantly alter reaction barriers and selectivity. Therefore, the addition of GC- or CP-DFT with continuum solvation and, where feasible, explicit electrolyte models can offer a more accurate representation of experimental electrochemical systems and hence provide a robust theoretical foundation for understanding potential-dependent reactivity in electrochemical C–N coupling reactions.

5.6. Transition-state calculations

While the free-energy diagram constructed from DFT calculations provides information about the thermodynamic feasibility of the intermediates, it does not indicate whether the specific reaction steps are kinetically accessible under experimental conditions. For electrocatalytic C–N coupling, transition state calculations are important, as steps such as C–N bond formation often compete with more kinetically favourable hydrogenation or ammonia formation pathways. The nudged elastic band (NEB) method is widely used to locate the minimum energy path and identify the geometry of the possible transition states between two stable states.[60,61]

NEB calculations, therefore, provide quantitative information on the kinetic barriers in the catalytic mechanism by identifying the activation energy and the nature of the transition state. For example, a study using NEB showed that differences in catalytic surfaces affect the barriers of the *NO + *CO coupling, which may be significantly lower than those for the sequential hydrogenation of *NO to *NH_2.[62] This explains the experimentally observed selectivity towards urea formation in Cu-based or bimetallic oxide catalysts. The transition state calculations may also provide further insight into the kinetic influence of defects or dopants, guiding the rational design of catalysts with a lower kinetic barrier to C–N bond formation.

5.7. Microkinetic modelling

Microkinetic modelling is the kinetic simulation of a reaction mechanism using elementary steps with rate constants, which is then solved to obtain reaction rates, surface coverages, and selectivity under steady-state or time-dependent conditions.[63] Microkinetic modelling involves both thermodynamic (ΔG) and kinetic parameters (activation energies) to derive the rate expressions for adsorption, desorption, surface reactions, PCET steps, and coupling reactions, and solve for coverages and rates self-consistently.

The surface coverage of the species i is defined as follows:

$$\theta_i = \frac{\text{number of sites occupied by species } i}{\text{total number of active sites}} \tag{12}$$

The number of empty sites is then defined by $\theta_* = 1 - \sum_i \theta_i$. The coverage evolution is written as follows:

$$\frac{d\theta_i}{dt} = (\text{rates that produce species } i) - (\text{rates that consume species } i) \tag{13}$$

Each elementary step (adsorption, desorption, reaction, diffusion, *etc.*) contributes to the coverage equations. All the coverage equations together form a system of coupled ordinary differential equations (ODEs) that is typically solved at steady state. An in-depth review of the use of microkinetic modelling for catalyst design has been published by Motagamwala and Dumesic.[64]

Applied to C–N coupling, microkinetic modelling can reveal how subtle changes in adsorption energies and barriers translate into current–potential behaviour, turnover frequencies, and product distributions. For instance, Xu *et al.* used microkinetic modelling to demonstrate that Co-Co- and Co-Ir-DACs can achieve higher current density (higher turnover frequency) at milder potentials, indicating that the DACs are more active for C–N coupling than Co-SAC. These results show the potential of microkinetic modelling to study the kinetics and macroscopic effects under steady-state conditions, which provides a

bridge from DFT energetics to experimentally relevant performance metrics.

5.8. *Ab Initio* molecular dynamics

Ab Initio Molecular Dynamics (AIMD) simulations enable time-resolved, atomistic simulation of catalytic interfaces at finite temperature, often in the presence of explicit solvent molecules.[65] AIMD goes one step further than static DFT by capturing the fluctuations in hydrogen bonding, solvent orientation, adsorption dynamics, and surface reconstruction. This is particularly useful in the study of C–N coupling as the key intermediates are sensitive to solvation structures and the proton-transfer network, which static DFT models cannot fully represent.

Several studies utilised AIMD simulations to assess catalyst stability under operating conditions, which can be critical for oxides, MXenes, COFs/MOFs and SACs. When external potentials are applied or the system temperature fluctuates, the catalyst surface may undergo reconstruction, resulting in a surface conformation different from that expected. In the study by Xiao *et al.* investigating the ability of Ru2-N6-C for the synthesis of urea, AIMD simulations were performed to test the kinetic stability at 300 and 500 K for 10 ps.[66] The simulations showed minimal fluctuation in energy, and the atomic position of the catalyst remains intact after the simulation period, indicating good dynamic structural stability, as shown in Fig. 3b.

5.9. Electronic structure analysis

The analysis of the electronic structure is essential for achieving a holistic understanding of the catalytic activity, selectivity, and reaction mechanism by revealing how adsorbates interact with the electronic states of the catalyst and how these interactions evolve along the reaction coordinate. Density of states (DOS) is the quantification of the number of quantum states in an energy interval that particles, such as electrons, are allowed to occupy.[68] A high DOS at a specific energy indicates a large number of states available for occupation. The DOS is important for understanding material properties, such as electrical conductivity and optical absorption. The projected density of states (pDOS) separates the total DOS into those for specific atoms or orbitals. The pDOS can show which atoms or orbitals contribute to the conduction or valence orbitals in the catalyst. An example of DOS analysis is shown in Fig. 3c and d, which shows the contribution of the elements and their respective orbitals to the total DOS.

Crystal orbital Hamilton population (COHP) analysis provides a quantitative measure of the bonding and anti-bonding interactions along specific bonds.[69,70] COHP separates the band-structure energy into orbital-pair interactions. It is akin to a DOS for specific bonds, in which both bonding and anti-bonding contributions are shown in the COHP diagram (Fig. 3c and d). For a specific interaction (*e.g.*, metal-adsorbate), if the COHP diagram shows a large positive peak far below the Fermi level, it indicates a strong bonding interaction, whereas a small negative peak just below the Fermi level indicates a weak anti-bonding interaction. Therefore, COHP diagrams can indicate whether certain interactions promote the stabilisation or destabilisation of the catalyst or catalyst–adsorbate system.

Bader charge analysis is another popular complementary technique for studying the electronic structure of catalysts, which involves partitioning the molecule's charge density into the respective atomic domains and determining the charge on each atom.[71,72] Using this analysis method, a better understanding of charge transfer between atoms during a reaction or interaction can be obtained, thereby correlating changes in charge with reaction energetics. This includes an increased knowledge of the type of bond formed during reactions or interactions.

6. Data-driven discovery

Having discussed some of the most common and well-established computational methods used for mechanistic studies, this section will focus on newer, data-driven methods that are becoming increasingly popular. Data-driven discovery refers to the use of quantitative data and computational or statistical models to guide the design of efficient catalysts, as well as their screening and optimisation, enabling catalyst design to occur more efficiently, rather than relying on intuition, trial-and-error, and excessive time-consuming, resource-intensive experimentation. Successful data-driven catalyst discovery relies on several significant factors. First, high-quality experimental data are important. This includes high-throughput screening and mechanistic information. Catalysts and their reactions are then described using descriptors or features. Some common descriptors include geometric descriptors (such as bond lengths and angles), electronic descriptors (such as charges and HOMO–LUMO energy levels), physicochemical descriptors (such as molecular weight or pK_a) and DFT-calculated descriptors (such as energy barriers or binding energy). Machine learning or statistical models, such as regression and Bayesian optimisation models, predict potential catalysts and conditions for specific reactions.

6.1. Machine learning and high-throughput mechanistic exploration

Recent advancements in catalyst discovery have driven a shift from manual trial-and-error DFT calculations to high-throughput screening and machine learning frameworks. The combination of these methods allows the framework to autonomously explore the chemical space of C–N coupling. In an example by Pan *et al.*, autonomous exploitation of reaction pathways was used to study the electrochemical C–N coupling on SACs. In this study, a graph-based, fully automated reaction-network exploration framework, which enables high-throughput mapping of all the possible intermediates and reaction pathways in C–N coupling on a SAC, was designed and constructed, as shown in Fig. 4a.[73] All possible intermediates and elementary steps involved in the C–N coupling on a Cu–N_4–C SAC were systematically enumerated. Molecules were represented as graphs, enabling high-throughput generation and screening of nearly 1500 intermediates and over 8000 elementary reactions.

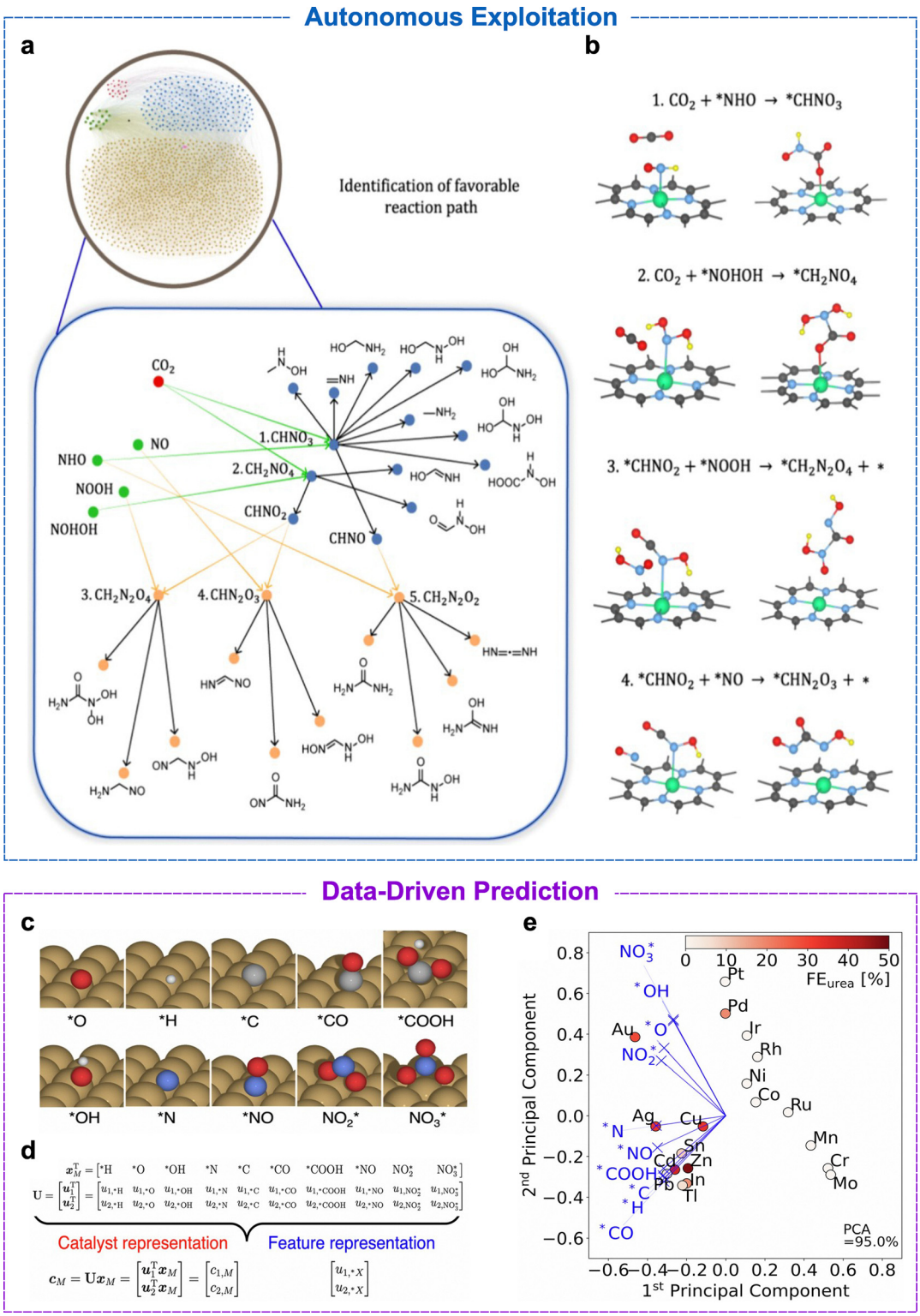

Fig. 4 Computational representations of the electrochemical C–N coupling pathways and catalyst-feature mapping. (a) Graphical representation of the reaction pathways involving C_1, N_1, C_1N_1, and C_1N_2 intermediates, shown as red, green, blue, and orange dots, respectively. Green lines indicate the coupling between C_1 and N_1 intermediates, while orange lines indicate the coupling between C_1N_1 and N_1 intermediates, leading to multiple possible C–N-containing products. (b) Initial and final configurations of the most common C–N coupling modes. Panels (a) and (b) are adapted from ref. 73, with permission from the American Chemical Society, copyright, 2024. (c) Ten distinct adsorption configurations considered for adsorbates on metal surfaces. (d) Schematic of the 10-dimensional vector x*M*, in which each component corresponds to an adsorption energy ΔE^*X, abbreviated as **X*. *U* is the projection operator, with u_1 and u_2 being the first two principal components. (e) Two-dimensional principal graph showing the feature representation in blue and the catalyst representation in red, with FE_{urea} indicated by colour sharing. The first two principal components capture 95% of the variance in the DFT energies. Panels (c), (d) and (e) are adapted from ref. 74, under the terms of the CC BY 4.0 license; the panels were reorganised and relabelled for clarity.

The resulting reaction network revealed that urea formation could proceed through more than 130 000 different pathways. High-throughput screening identified 813 stable surface intermediates, which bind not only to the Cu centre but also to adjacent C and N atoms, indicating that the support can also act as an active site to promote C–N bond formation. The study demonstrated that C–N coupling preferentially occurs between CO_2 and nitrogen-containing intermediates rather than through *COOH, as the formation of *COOH from CO_2 is energetically unfavourable with a barrier of 1.60 eV. It was also shown that more highly hydrogenated nitrogen species, particularly $*NH_2$, have lower C–N coupling barriers.

The framework was extended to 38 $M–N_x–C$ SACs, and the authors identified $Mo–N_3–C$, $W–N_3–C$, and $Sb–N_3–C$ as promising catalysts that balance CO_2 activation with $*NH_2$ stabilisation. Overall, this work demonstrates the capability of automated graph-based reaction-network exploration in uncovering complex C–N coupling mechanisms, thereby guiding the rational design of SACs.

6.2. Descriptor-based predictions and statistical dimensionality reduction

Recent data-driven studies use physical descriptors to rationalise reactivity trends and help accelerate catalyst discovery. In a study by Yodsin *et al.*, a comprehensive DFT screening of 26 transition-metal SACs supported on graphitic C_2N ($M@C_2N$) was conducted for electrochemical urea synthesis from N_2 and CO_2 under ambient conditions.[67] The study detailed a descriptor strategy that links electronic structure to catalytic performance. Four pathways, CO_2, OCOH, CO, and NCON routes, were accessed mechanistically, and the initial N_2 protonation and the final hydrogenation steps were identified as the most energy-demanding steps, which determine the activity of the catalyst. The three transition metals, Nb, Mo, and Re, exhibited low limiting potentials of $\approx$0.5 V, making them promising catalysts for urea synthesis. The paper proposes a predictive descriptor, Φ, which incorporates the d-electron count and the electronegativity of the metal centre. The descriptor shows a good correlation with the calculated limiting potentials across the 26 transition metals, thereby enabling accurate prescreening before the calculation of the full pathway and saving computational expense.

In contrast to the mechanistic approach of Yodsin *et al.*, Wuttke and Bagger adopted a data-driven approach based on experimentally measured urea faradaic efficiencies for CO_2 and nitrite co-reduction, without assuming a fully resolved mechanism.[74] Principal component analysis (PCA), an unsupervised machine learning algorithm, of selectivity data revealed that urea formation correlates strongly with concurrent CO and NH_3 production. The adsorption energies of ten intermediates on nineteen transition metals were used to construct a descriptor space, with the first two principal components capturing 95% of the variance. From this analysis, the adsorption energies, ΔE_{*H} and ΔE_{*O}, were identified as key descriptors representing hydrogen evolution suppression and oxophilicity, respectively. While ΔE_{*H} showed a weak positive correlation with urea selectivity, strong oxygen binding (ΔE_{*O}) was found to be favourable.

These studies illustrate how both mechanistically motivated descriptors and statistical dimensionality reduction can identify

Table 1 Comparison of the computational strategies for electrochemical C–N coupling

Computational approach	Primary advantages	Key limitations	Best use conditions
Periodic DFT	To obtain accurate simulation of infinite crystalline lattices and their surfaces. Enables the calculation of electronic structure data	High computational cost for large cells. Typically uses fixed electron counts and vacuum conditions	Used for initial mechanistic screening, calculating the adsorption energies and properties of bulk systems
Computational hydrogen electrode	Computationally efficient, allowing the evaluation of potential-dependent PCET steps without explicit solvation	Purely thermodynamic; does not consider kinetic barriers, explicit charge transfer, and potential-dependent solvation	Used in the construction of free-energy diagrams and identifying potential-determining steps in aqueous media
Grand-canonical DFT	Mimics experimental conditions by allowing electron fluctuation, thereby capturing the potential-dependent electrostatic effects	Computationally expensive compared with standard periodic DFT or CHE	Investigating interfacial electric-field effects on transition states or comparing the effects of applied potential on catalyst efficiency
Solvation models	Implicit: Captures long-range polarisation effects Hybrid: Captures local hydrogen-bonding and proton-transfer	Implicit: Models lack explicit donor/acceptor behaviour Hybrid: Models result in an increase in computational cost	Simulating the solid–liquid interface when the solvent may have a significant influence on the studied reaction
Microkinetic modelling	Provides a bridge between DFT energetics and experimental results, such as current density and turnover frequency	Accuracy is highly dependent on the quality of DFT parameters	Used for predicting macroscopic performance and identifying kinetic bottlenecks under steady-state conditions
Machine learning and high-throughput screening	Enables autonomous and rapid exploration of vast chemical spaces and complex reaction networks	Requires high-quality datasets, with its reliability limited by the descriptors and training models used	Used for the discovery of new catalyst candidates and identifying universal descriptors for large material libraries

the key physicochemical factors governing selectivity, even when the explicit reaction pathway remains uncertain. Several other papers use similar approaches to identify descriptors.[75,76] While the descriptors may vary, descriptor-based predictions provide a powerful toolkit for accelerating efficient catalyst disco

6.3. Comparative analysis of computation frameworks

The selection and use of appropriate computational methods are critical factors in modelling electrochemical C–N coupling, as a balance between chemical accuracy and computational feasibility must be achieved. While periodic DFT provides a foundational understanding of the solid-state catalyst, additional methods, such as GC-DFT and explicit solvation models, may be required to form a more holistic understanding of the reaction mechanism and properties of the system. To assist in the navigation of these methodologies, Table 1 provides a comparative overview of the computational strategies discussed, specifying their strengths and limitations, as well as the events in which they are most effectively applied.

7. Conclusion and Future outlook

Electrochemical C–N coupling offers a promising pathway for converting CO_2 and nitrogen-containing feedstocks into value-added chemicals under ambient conditions, providing sustainable alternatives to the traditional thermochemical processes. Despite the different catalyst classes, some challenges remain common, including balancing the adsorption strengths of key intermediates, enabling their coupling while suppressing competitive pathways. Computational chemistry has played a pivotal role in achieving these requirements. Applying periodic DFT with improved models to mimic experimental conditions has provided insights into surface energetics and elucidated the reaction mechanism. AIMD simulations have enabled the study of the dynamic behaviour of the catalytic interface and the stability under realistic conditions, while transition state calculations and microkinetic modelling have provided insights into the kinetic factors governing C–N bond formation. The collaboration between computational innovation and experimental results has enabled more rational catalyst-design strategies and provided deeper insights into selectivity trends, leading to rapid progress in the field. However, despite the rapid progress, challenges and opportunities remain for electrochemical C–N coupling. Most studies remain catalyst-class specific, and a generalised framework that studies the mechanisms and selectivity is still lacking. The development of universal descriptors that capture sufficient information, regardless of the catalyst, would accelerate the screening of different catalysts. Another area of development is the interaction of experiment and computational feedback. Many autonomous and data-driven techniques require large amounts of well-organised data, which also presents as a bottleneck to the development of efficient data-driven discoveries, necessitating improved standardisation and closer alignment between the reporting of experimental practices and computation requirements to enable reliable model training and validation.

Author contributions

J. L. performed the analysis of literature, preparation of figures, and writing of the manuscript, and P. O. provided supervision and guidance for the overall structure and revision of the paper.

Conflicts of interest

There are no conflicts to declare.

Data availability

Data availability is not applicable to this article as no new data were created or analysed in this study.

Acknowledgements

We acknowledge the support from NUS Industry-Relevant PhD Scholarship.

References

1 I. Santos Mesquita, P. Albuquerque Melo and A. Resende Secchi, *Appl. Energy*, 2025, **400**, 126527.
2 W. Z. Chen, H. Su, X. P. Chen, X. Zheng, J. Tang, Y. Li, Q. X. Wang and Y. Ling, *ACS Sustain. Chem. Eng.*, 2025, **13**, 18367–18376.
3 A. Adalder, K. Mitra, N. Barman, R. Thapa, R. Urkude, S. Das and U. K. Ghorai, *Small*, 2025, **21**, 2505313.
4 H. J. Fang, C. H. Kuo, H. S. Yang, Z. Wang, X. Z. Feng, W. J. Ji and C. T. Au, *Green Chem.*, 2024, **26**, 6812–6821.
5 X. Q. Li, Y. Y. Li, H. Q. Li, W. K. Li, Y. J. Cheng, H. P. Lin, W. J. Huang and S. Y. Xiong, *ACS Nano*, 2025, **19**, 33485–33495.
6 T. Liu, Y. Wang and Y. Li, *JACS Au*, 2023, **3**, 943–952.
7 C. Tang, L. Chen, H. Li, L. Li, Y. Jiao, Y. Zheng, H. Xu, K. Davey and S.-Z. Qiao, *J. Am. Chem. Soc.*, 2021, **143**, 7819–7827.
8 J. J. Hu, S. Osella, J. Albero and H. Garcia, *EES Catal.*, 2025, **3**, 1075–1086.
9 R. Yu, T. F. Xu, Z. R. Liu, D. Legut, J. W. Sun, J. S. Francisco and R. F. Zhang, *Small*, 2025, **21**, 2502091.
10 X. R. Zhu, X. C. Zhou, Y. Jing and Y. F. Li, *Nat. Commun.*, 2021, **12**, 4080.
11 A. Bairagi, A. Y. Pereverzev, P. Tinnemans, E. A. Pidko and J. Roithová, *J. Am. Chem. Soc.*, 2024, **146**, 5480–5492.
12 S. B. Patil, C. R. Lee, S. M. Gowdru, C. C. Chang, S. T. Chang, Y. C. Chen, K. C. Wu, C. C. Chang, S. C. Haw and D. Y. Wang, *J. Mater. Chem. A*, 2023, **11**, 11495–11506.
13 Z. Y. Li, J. Xiong, W. Dong, Y. F. Huang, S. C. Liu, Y. Q. Huang, Y. Mao, Z. W. Liang and X. Luo, *Sep. Purif. Technol.*, 2023, **325**, 124544.
14 G. Leonzio, A. Hankin and N. Shah, *Chem. Eng. Res. Des.*, 2024, **208**, 934–955.
15 B. M. Hoffman, D. Lukoyanov, Z.-Y. Yang, D. R. Dean and L. C. Seefeldt, *Chem. Rev.*, 2014, **114**, 4041–4062.
16 S. Garcia-Segura, M. Lanzarini-Lopes, K. Hristovski and P. Westerhoff, *Appl. Catal., B*, 2018, **236**, 546–568.
17 L. Yue, W. Song, L. Zhang, Y. Luo, Y. Wang, T. Li, B. Ying, S. Sun, D. Zheng, Q. Liu, A. Farouk, M. S. Hamdy, S. Alfaifi and X. Sun, *Small Struct.*, 2023, **4**, 2300168.
18 J. Leverett, T. Tran-Phu, J. A. Yuwono, P. Kumar, C. Kim, Q. F. Zhai, C. Han, J. T. Qu, J. Cairney, A. N. Simonov, R. K. Hocking, L. M. Dai, R. Daiyan and R. Amal, *Adv. Energy Mater.*, 2022, **12**, 2201500.

19 X. D. Xuan, K. Y. Jiang, S. H. Huang, B. X. Feng, F. Qiu, S. Han, J. H. Zhu and X. D. Zhuang, *J. Mater. Sci.*, 2022, **57**, 10129–10140.
20 Y. Wan, M. Zheng, W. Yan, J. Zhang and R. Lv, *Adv. Energy Mater.*, 2024, **14**, 2303588.
21 D. X. Jiao, Z. X. Wang, Y. J. Liu, Q. H. Cai, J. X. Zhao, C. R. Cabrera and Z. F. Chen, *Energy Environ. Mater.*, 2024, **7**, e12496.
22 Y. Y. Cao, Y. X. Meng, Y. T. Wu, H. J. Huang, W. C. Zhong, Z. F. Shen, Q. N. Xia, Y. G. Wang and X. Li, *J. Mater. Chem. A*, 2022, **10**, 23843–23853.
23 Y. Y. Cao, Y. X. Meng, R. Z. An, X. H. Zou, H. J. Huang, W. C. Zhong, Z. F. Shen, Q. E. Xia, X. Li and Y. A. Wang, *J. Colloid Interface Sci.*, 2023, **641**, 990–999.
24 A. Lasia, *Int. J. Hydrogen Energy*, 2019, **44**, 19484–19518.
25 M. Khalil, G. T. M. Kadja, F. A. A. Nugroho, L. G. Sutanto, P. K. Jiwanti, F. F. Abdi, F. Hussin and M. K. Aroua, *Renewable Sustainable Energy Rev.*, 2024, **206**, 114869.
26 W. W. Hong, J. B. Jakobsen, D. Golo, M. R. Madsen, M. S. G. Ahlquist, T. Skrydstrup, S. U. Pedersen and K. Daasbjerg, *ChemElectroChem*, 2024, **11**, e202300553.
27 C. Li, Y. Wang, C. Wang, Q. M. Wu, X. Y. Lv, S. X. Xie, L. C. Kong, J. J. Feng, Z. Q. Li, A. J. Wang, J. W. Kang and F. Yang, *ACS Appl. Mater. Interfaces*, 2025, **17**, 26594–26603.
28 J. T. Feaster, C. Shi, E. R. Cave, T. Hatsukade, D. N. Abram, K. P. Kuhl, C. Hahn, J. K. Nørskov and T. F. Jaramillo, *ACS Catal.*, 2017, **7**, 4822–4827.
29 Y. Zhao, J. Zhang, X. Guo, X. Cao, S. Wang, H. Liu and G. Wang, *Chem. Soc. Rev.*, 2023, **52**, 3215–3264.
30 S. Zhou, X. Yang, W. Pei, Z. Jiang and J. Zhao, *J. Phys.: Energy*, 2021, **3**, 012002.
31 M. Y. Cong, Q. Liu, D. P. Wang, S. J. Hao, Z. Z. Han, H. E. Xu, M. X. Guo, X. Ding and Y. Gao, *Appl. Catal., B*, 2024, **351**, 123941.
32 K. Yu, H. Wang, W. Yu, Z. Zhang and Z. Bian, *Chem. Eng. J.*, 2025, **514**, 163048.
33 Q.-Y. Li, Y. Quan, W. Wei, J. Li, H. Lu, R. Ni and X.-J. Wang, *Polyhedron*, 2015, **99**, 1–6.
34 X. M. Yuan, D. M. F. Xiao, C. L. Zhao and C. L. Zhang, *Small*, 2025, **21**, 2411316.
35 T. Sun, J. Wu, X. Lu and X. Tang, *Mol. Catal.*, 2024, **559**, 114047.
36 J. Li and N. Kornienko, *Chem. Sci.*, 2022, **13**, 3957–3964.
37 Y. Zhao, Y. Ding, W. Li, C. Liu, Y. Li, Z. Zhao, Y. Shan, F. Li, L. Sun and F. Li, *Nat. Commun.*, 2023, **14**, 4491.
38 P. Ramadhany, T. Tràn-Phú, J. A. Yuwono, Z. P. Ma, C. Han, T. K. A. Nguyen, J. Leverett, P. Kumar, R. K. Hocking, A. Tricoli, A. N. Simonov, R. Amal and R. Daiyan, *Adv. Energy Mater.*, 2024, **14**, 2401786.
39 Y. J. Hou and L. Guo, *Catal. Surv. Asia*, 2024, **28**, 117–133.
40 Y. Tan, X. K. Chen, J. Yuan, G. Sheng, W. Q. Deng and H. Wu, *Angew. Chem., Int. Ed.*, 2025, **64**, e202513441.
41 Y. Liu, Z. Zeng, R. Peng, K. Ma, Y. Li and Z. Yan, *Sci. Rep.*, 2025, **15**, 20619.
42 J. R. Du, H. H. Wang, C. W. Yue, I. A. Soomro, M. Pu and M. Lei, *Appl. Surf. Sci.*, 2024, **658**, 159854.
43 Y. J. Hou, L. Guo and F. L. Luo, *Catal. Surv. Asia*, 2023, **27**, 363–378.
44 M. Karamad, *ACS Catal.*, 2025, **15**, 8497–8510.
45 W. C. Zhong, D. X. Chen, Y. T. Wu, J. X. Yue, Z. F. Shen, H. Huang, Y. A. Wang, X. Li, J. P. Lang, Q. E. Xia and Y. Y. Cao, *J. Colloid Interface Sci.*, 2024, **655**, 80–89.
46 B. Hammer, L. B. Hansen and J. K. Nørskov, *Phys. Rev. B:Condens. Matter Mater. Phys.*, 1999, **59**, 7413–7421.
47 I. Grinberg, Y. Yourdshahyan and A. M. Rappe, *J. Chem. Phys.*, 2002, **117**, 2264–2270.
48 J. Sun, A. Ruzsinszky and J. P. Perdew, *Phys. Rev. Lett.*, 2015, **115**, 036402.
49 R. B. Araujo, G. L. S. Rodrigues, E. C. dos Santos and L. G. M. Pettersson, *Nat. Commun.*, 2022, **13**, 6853.
50 C. Adamo and V. Barone, *J. Chem. Phys.*, 1999, **110**, 6158–6170.
51 S. M. R. Islam, F. Khezeli, S. Ringe and C. Plaisance, *J. Chem. Phys.*, 2023, **159**, 234117.
52 O. Andreussi, I. Dabo and N. Marzari, *J. Chem. Phys.*, 2012, **136**, 064102.
53 A. Okur and C. Simmerling, in *Annual Reports in Computational Chemistry*, ed. D. C. Spellmeyer, Elsevier, 2006, vol. 2, pp. 97–109.
54 J. K. Nørskov, J. Rossmeisl, A. Logadottir, L. Lindqvist, J. R. Kitchin, T. Bligaard and H. Jónsson, *J. Phys. Chem. B*, 2004, **108**, 17886–17892.
55 A. Rendón-Calle, S. Builes and F. Calle-Vallejo, *Curr. Opin. Electrochem.*, 2018, **9**, 158–165.
56 M. M. Melander, M. J. Kuisma, T. E. K. Christensen and K. Honkala, *J. Chem. Phys.*, 2018, **150**, 041706.
57 K. Letchworth-Weaver and T. A. Arias, *Phys. Rev. B:Condens. Matter Mater. Phys.*, 2012, **86**, 075140.
58 C. Y. Zhu, Y. Geng, X. H. Yao, G. S. Zhu, Z. M. Su and M. Zhang, *Small Methods*, 2023, **7**, 2201331.
59 H. C. Li, Y. S. Ho, G. L. Yang, R. H. Li, T. C. Kuo, C. T. Hsieh, Y. Kwon and M. J. Cheng, *J. Phys. Chem. C*, 2024, **128**, 1058–1067.
60 G. Henkelman and H. Jónsson, *J. Chem. Phys.*, 2000, **113**, 9978–9985.
61 G. Henkelman, B. P. Uberuaga and H. Jónsson, *J. Chem. Phys.*, 2000, **113**, 9901–9904.
62 T. Z. Xu, Z. F. Wang, T. Y. Liu, F. F. Wang and Y. Jing, *J. Am. Chem. Soc.*, 2025, **147**, 26969–26979.
63 P. Stoltze, *Prog. Surf. Sci.*, 2000, **65**, 65–150.
64 A. H. Motagamwala and J. A. Dumesic, *Chem. Rev.*, 2021, **121**, 1049–1076.
65 M. P. Allen, *Computer simulation of liquids*, Clarendon Press, USA, 1989.
66 T. Xiao, C. M. Tang, F. Xion and Y. Y. Wang, *Mol. Catal.*, 2025, **586**, 115440.
67 N. Yodsin, T. Potale, Y. Injongkol, P. Pimbaotham and S. Namuangruk, *J. Mater. Chem. A*, 2025, 13.
68 C. Kittel, *Introduction to Solid State Physics*, Wiley, 2004.
69 R. Dronskowski and P. E. Bloechl, *J. Phys. Chem.*, 1993, **97**, 8617–8624.
70 V. L. Deringer, A. L. Tchougréeff and R. Dronskowski, *J. Phys. Chem. A*, 2011, **115**, 5461–5466.
71 C. Kittel, *Atoms in Molecules - A Quantum Theory*, Oxford University Press, 1990.
72 G. Henkelman, A. Arnaldsson and H. Jónsson, *Comput. Mater. Sci.*, 2006, **36**, 354–360.
73 J. J. Pan, H. W. Ding, X. Z. Yang, X. H. Liang, S. L. Wu, M. Z. Zhang, S. N. Li, S. S. Zheng and F. Pan, *ACS Catal.*, 2024, **15**, 457–467.
74 A. Wuttke and A. Bagger, *Comm. Chem.*, 2025, **8**, 30.
75 Z. W. Xiong, Y. Xiao and C. Shen, *Chem. Mater.*, 2022, **34**, 9402–9413.
76 Y. Xiao, C. Shen, C. Sun, Y. B. Yang, X. Yang and L. L. Han, *ACS Appl. Mater. Interfaces*, 2024, **16**, 12486–12499.

